Dynamics and instability of nonlinear Fano resonances in photonic crystals

Andrey E. Miroshnichenko and Yuri Kivshar
Nonlinear Physics Centre and Centre for Ultra-high-bandwidth Devices for Optical Systems (CUDOS), Research School for Physics and Engineering, Australian National University, Canberra ACT 0200, Australia

Christoph Etrich and Thomas Pertsch
Institute of Applied Physics/Ultra Optics, Friedrich-Schiller-Universität Jena, Max-Wien-Platz 1, 07743 Jena, Germany

Rumen Iliew and Falk Lederer
Institute of Condensed Matter Theory and Solid State Optics, Friedrich-Schiller-Universität Jena, Max-Wien-Platz 1, 07743 Jena, Germany

(Received 20 August 2008; published 12 January 2009)

We employ an effective discrete model for the study of wave propagation in a photonic crystal waveguide side-coupled to a cavity with Kerr-type nonlinearity. Taking into account the linear coupling between guided and localized states and applying the time-dependent version of a Green's function formalism, we study and characterize analytically the scattering of continuous waves. The resonant reflectivity, which is tunable via the nonlinearity, takes the form of a *nonlinear Fano resonance* because the output field is composed of a linearly transmitted wave and a resonantly reflected contribution from the localized cavity. By studying the stability of the nonlinear Fano resonance, we reveal that the continuous-wave scattering may exhibit *modulational instability* near the resonance when the light intensity in the cavity starts growing in time. However, we demonstrate that this instability may be suppressed for Gaussian pulses, such that the bistable transmission curve can still be recovered in accordance with the analysis of the steady-state transmission. We demonstrate that our analytical results based on an effective discrete model are in excellent agreement with numerical results obtained by direct finite-difference time-domain simulations.

DOI: 10.1103/PhysRevA.79.013809 PACS number(s): 42.65.Sf, 42.65.Pc

I. INTRODUCTION

One of the simplest bistable optical devices that might be employed in future photonic integrated circuits is a nonlinear two-port structure which is connected to other parts of a circuit by one input and one output waveguide. The transmission properties of this nonlinear device depend on the light intensity coupled into the input waveguide. One of the realizations of such a device is provided by a waveguide side-coupled to an optical cavity. This system is known to exhibit a Fano resonance in reflection, and it also demonstrates optical bistability when the cavity is made of a nonlinear material [1,2].

In such systems the Fano resonance originates from the coupling between discrete (localized) and continuum (extended) states, and it manifests itself as constructive or destructive interference phenomena. It is widely known across different branches of physics as the appearance of resonant asymmetric profiles in transmission or absorption spectra observed in numerous physical systems, including light absorption by atomic systems [3], the Aharonov-Bohm interferometer [4,5], quantum dots [6–8], light propagation through a variety of configurations in photonic circuits [1,9–21], phonon scattering by time-periodic scattering potentials [22–24].

Possible realizations of photonic crystal devices based on Fano resonances have been demonstrated in recent experiments with both linear and nonlinear light transmission in two-dimensional photonic crystal slab structures where a lattice of cylindrical pores is etched into a planar waveguide. In particular, the Noda group demonstrated coupling of a photonic crystal waveguide to a leaky resonator mode consisting of a defect pore of slightly increased radius [25,26]. Notomi *et al.* [27] and Barclay *et al.* [28] observed all-optical bistability in directly coupled photonic-crystal waveguide-resonator systems. More recently, Yang *et al.* [29] demonstrated experimentally Fano-resonance-enhanced bistability in a side-coupled geometry.

The main objective of this paper is to study the dynamics and instabilities of the nonlinear Fano resonance in photonic crystals. First, we develop a time-dependent version of the Green's function formalism and study the temporal dynamics in the photonic-crystal structure composed of a straight waveguide and a side-coupled cavity with Kerr-type nonlinearity. In particular, we reveal the existence of modulational instability near the resonance that is manifested as a growth of the light intensity inside the cavity. Second, we study, both analytically and numerically, the manifestation of the nonlinear Fano resonance for pulse propagation. In particular, we demonstrate that, in spite of the predicted modulational instability of the continuous waves, the instability can be suppressed for pulse propagation, such that it becomes possible to recover the bistable transmission curves of the stationary scattering with an excellent agreement with numerical results obtained by finite-difference time-domain (FDTD) simulations, where Maxwell's equations are discretized in space and time without further approximations [30].

The paper is organized as follows. In Sec. II we generalize the Green's function formalism for describing photonic crystal circuits in the nonstationary case, in order to analyze both instabilities and pulse scattering. Section III is devoted to the derivation of the effective discrete equations for the resonant interaction between a straight waveguide and an

isolated side-coupled nonlinear defect, where we also introduce and discuss the appropriate boundary conditions. In Sec. IV we analyze the stability of the nonlinear Fano resonance scattering and reveal that the system shows a modulational instability near the resonance. The problem of pulse scattering is analyzed in Sec. V where we also compare our analytical solutions to the numerical results obtained by FDTD calculations. Finally, Sec. VI concludes the paper.

II. GREEN'S FUNCTION FORMALISM

As already shown earlier [31,32], the Green's function approach allows one to obtain very accurate results compared to more time-consuming direct numerical FDTD simulations, even for rather complex geometries of the photonic circuits. Here we develop a generalization of this approach, taking into account the explicit temporal dependences, which permits the study of pulse propagation and scattering.

We consider a periodic square lattice of infinite cylindrical rods parallel to the z axis. We neglect the material dispersion and assume the dielectric constant $\epsilon(\vec{r})$ to be periodic in two transverse directions with period a, $\vec{r}=(x,y)$. In this geometry, the evolution of the E-polarized electric field propagating in the (x,y) plane is governed by the scalar wave equation

$$\nabla^2 E_z(\vec{r},\tau) - \frac{1}{c^2}\partial_\tau^2[\epsilon(\vec{r})E_z(\vec{r},\tau)] = 0, \tag{1}$$

where $\nabla^2=\partial_x^2+\partial_y^2$. The light field propagating in such structures can be separated into fast and slow components, $E_z(\vec{r},\tau)=e^{-i\omega\tau}E(\vec{r},\tau|\omega)$, where $E(\vec{r},\tau|\omega)$ is a slowly varying envelope of the electric field—i.e., $\partial_\tau^2 E(\vec{r},\tau|\omega) \ll \omega\partial_t E(\vec{r},\tau|\omega)$. This allows one to simplify Eq. (1) to the form

$$\left[\nabla^2 + \epsilon(\vec{r})\left(\frac{\omega}{c}\right)^2\right]E(\vec{r},\tau|\omega) \simeq -2i\epsilon(\vec{r})\frac{\omega}{c^2}\frac{\partial E(\vec{r},\tau|\omega)}{\partial\tau}. \tag{2}$$

Both the straight waveguide and the side-coupled cavity are created by introducing defect rods into a perfect two-dimensional periodic structure, as shown in Fig. 1(a). Therefore, the dielectric constant can be represented as a sum of two contributions, describing the periodic and defect structures $\epsilon(\vec{r})=\epsilon_{\rm pc}+\delta\epsilon$. We employ the Green's function of the two-dimensional periodic structure without defects, which can be found from the equation

$$\left[\nabla^2 + \epsilon_{\rm pc}(\vec{r})\left(\frac{\omega}{c}\right)^2\right]G(\vec{r},\vec{r}'|\omega) = -\delta(\vec{r}-\vec{r}'), \tag{3}$$

and rewrite Eq. (2) in the integral form

$$E(\vec{r},\tau|\omega) = \int d^2\vec{r}'\, G(\vec{r},\vec{r}'|\omega)\hat{L}E(\vec{r}',\tau|\omega), \tag{4}$$

where we have introduced the linear operator

$$\hat{L} = \left(\frac{\omega}{c}\right)^2\delta\epsilon(\vec{r}) + 2i\epsilon(\vec{r})\frac{\omega}{c^2}\frac{\partial}{\partial\tau}, \tag{5}$$

and consider the time evolution of the slowly varying envelope as a perturbation to the steady state.

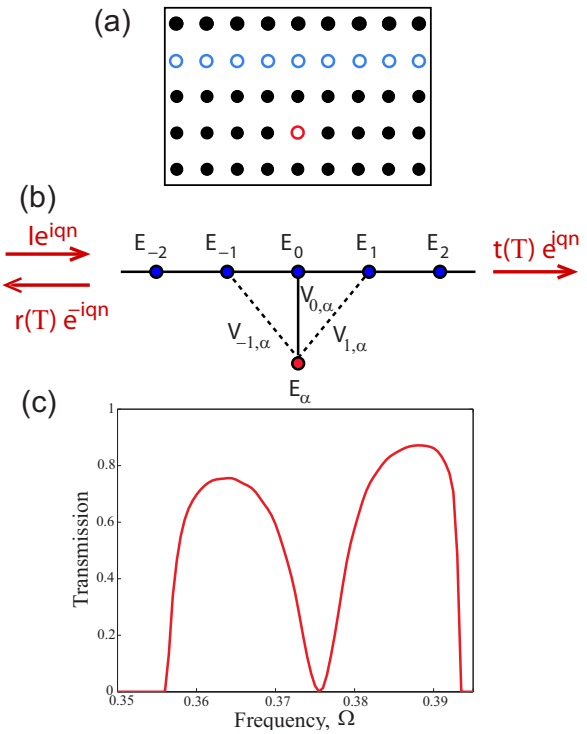

FIG. 1. (Color online) Schematic view of (a) the photonic crystal waveguide with an isolated side-coupled *nonlinear* cavity and (b) the effective discrete system (8). (c) Typical profile of the linear Fano resonance in such a system. The resonant frequency is $\Omega=0.3765$. Here and in the following we introduced the normalized frequency $\Omega=a/\lambda$.

The defect rods introduced into the periodic structure can formally be described as follows:

$$\delta\epsilon(\vec{r}) = \sum_{n,m}[\delta\epsilon_{m,n}^{(0)} + \chi^{(3)}|E(\vec{r},\tau|\omega)|^2]\theta(\vec{r}-\vec{r}_{n,m}), \tag{6}$$

where we use the θ function to describe the position of a defect rod at site n,m, where $\theta(\vec{r})=1$ for $\vec{r}$ inside the defect rods and $\theta(\vec{r})=0$ otherwise, and $\delta\epsilon_{m,n}^{(0)}$ is the variation of the dielectric constant of the defect rod (m,n). Importantly, this approach allows us to incorporate a nonlinear response in a straightforward manner, which is assumed as a Kerr nonlinearity described by $\chi^{(3)}|E|^2$.

Substituting Eq. (6) into the integral equation (4) and assuming that the electric field does not change inside the dielectric rods, we can evaluate the integral on the right-hand side of Eq. (4) and derive a set of *discrete nonlinear equations*

$$i\sigma\frac{\partial}{\partial\tau}E_{n,m} - E_{n,m} + \sum_{k,l}J_{n-k,m-l}(\omega)(\delta\epsilon_{k,l}^{(0)} + \chi^{(3)}|E_{k,l}|^2)E_{k,l} = 0, \tag{7}$$

for the amplitudes of the electric field $E_{n,m}(\tau|\omega)=E(\vec{r}_{n,m},\tau|\omega)$ calculated at the defect rods. The parameters σ and $J_{k,l}(\omega)$ are determined by using the corresponding integrals of the Green's function, where the whole information about the photonic crystal dispersion is now hidden in their

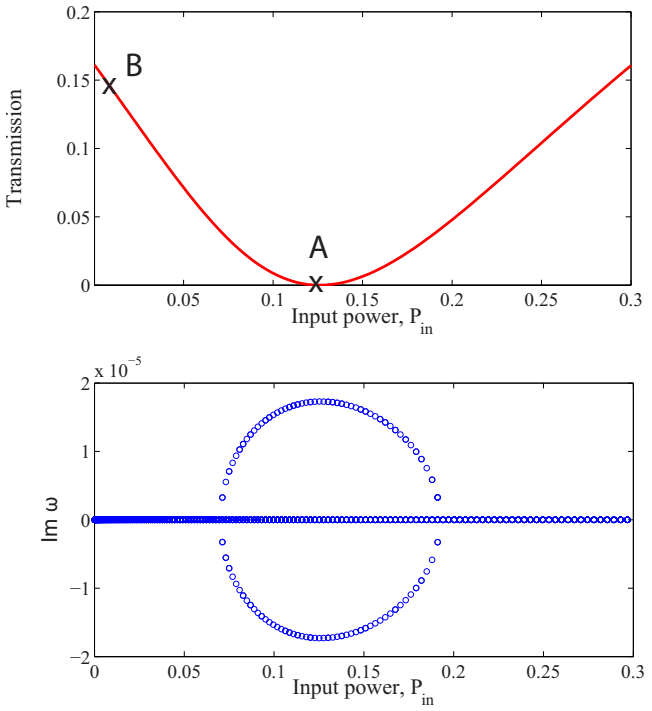

FIG. 2. (Color online) (a) Nonlinear transmission coefficient and (b) imaginary part of eigenvalues of the linearized system vs input power. The permittivities of the side-coupled defect and defect rods are $\epsilon_n=\epsilon_\alpha=2.56$. The frequency of the incoming continuous wave is $\Omega=0.3785$ [see Fig. 1(c)]. It shows that near the nonlinear Fano resonance the continuous wave becomes dynamically unstable.

specific frequency dependencies, which can be found in Refs. [2,33]. In this way, the Green's function (3) needs to be calculated only once for a given photonic structure—e.g., by employing the approach outlined in Ref. [34]—and then it can be used to study any photonic circuit in that structure.

III. WAVEGUIDE WITH A COUPLED DEFECT

We study the transmission properties of a photonic crystal waveguide with a side-coupled nonlinear defect, as shown in Fig. 1(a). This problem was studied earlier for the stationary resonant transmission [2,35], and it was demonstrated that this structure exhibits bistable transmission even for low input powers. In this paper, we reexamine this problem by considering the time-dependent evolution. For this geometry, the dynamical equations (7) can be written as follows:

$$-i\sigma\frac{\partial}{\partial T}E_n=\sum_{k=1}^{L}V_{0,k}(\Omega)(E_{n-k}+E_{n+k})-D_n(\Omega)E_n+\sum_{l=n_1}^{n_2}\delta_{n,l}V_{l-n_1,\alpha}E_\alpha,$$

$$-i\sigma\frac{\partial}{\partial T}E_\alpha=\kappa_\alpha(\Omega)|E_\alpha|^2E_\alpha-D_\alpha(\Omega)E_\alpha+\sum_{l=n_1}^{n_2}V_{\alpha,l-n_1}E_l, \tag{8}$$

where $V_{n,m}(\Omega)=\delta\epsilon_m J_{n,m}(\Omega)$, $D_n(\Omega)=1-\delta\epsilon_n J_{0,0}(\Omega)$, $D_\alpha(\Omega)=1-\delta\epsilon_\alpha J_{0,0}(\Omega)$, and $\kappa_\alpha(\Omega)=\chi_\alpha^{(3)}J_{0,0}(\Omega)$ and the normalized

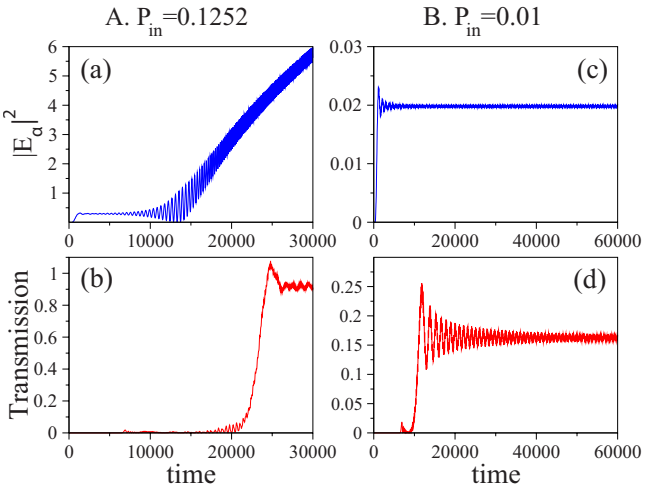

FIG. 3. (Color online) (a),(c) Temporal evolution of the electric field in the cavity and (b),(d) transmission coefficient for two different values of the input power: (a),(b) at resonance, $P_{\text{in}}=0.1252$, and (c),(d) far from the resonance, $P_{\text{in}}=0.01$. Near the resonance the dynamics of the field in the cavity shows the development of a modulational instability of continuous-wave scattering.

frequency and time have been introduced as $\Omega=a/\lambda$, and $T=2\pi c/a\tau$, respectively. The side-coupled defect is situated in the middle of the structure near the site $n=0$, where we take into account the nonlocal coupling to the straight PC waveguide with $n_1=-1$ and $n_2=1$ [see Fig. 1(b)].

To study the transmission properties of the system, we impose the scattering boundary conditions

$$E_n(T|\Omega)=\begin{cases}Ie^{iq(\Omega)n}+r(T)e^{-iq(\Omega)n}, & n\ll 0,\\ t(T)e^{iq(\Omega)n}, & n\gg 0,\end{cases} \tag{9}$$

which depend slowly on time.

It is known that in photonic-crystal waveguides the effective interaction between defect rods is long range [32,36] and, thus, in general, we should have $L>1$. However, the coupling strength decays exponentially with the distance and, as a result, for coupled-resonator optical waveguides (CROWs) the specific discrete array with nearest-neighbor interactions ($L=1$) gives already excellent agreement with direct FDTD simulations [32]. Therefore, we will use this approximation for our dynamical model (8) taking $L=1$.

We use the linear substitution $E_n=e^{i\nu T}\tilde{E}_n$ with $\nu=-D_n(\omega)/\sigma$ in Eq. (7) to eliminate $D_n(\omega)$ and obtain

$$-i\sigma\frac{\partial}{\partial T}\tilde{E}_n=V_{0,1}(\Omega)(\tilde{E}_{n-1}+\tilde{E}_{n+1})+\sum_{l=n_1}^{n_2}\delta_{n,l}V_{l-n_1,\alpha}E_\alpha,$$

$$-i\sigma\frac{\partial}{\partial T}\tilde{E}_\alpha=\kappa_\alpha(\Omega)|\tilde{E}_\alpha|^2\tilde{E}_\alpha+[D_n(\Omega)-D_\alpha(\Omega)]\tilde{E}_\alpha+\sum_{l=n_1}^{n_2}V_{\alpha,l-n_1}E_l. \tag{10}$$

Accordingly, the scattering boundary conditions for the electric fields take the form

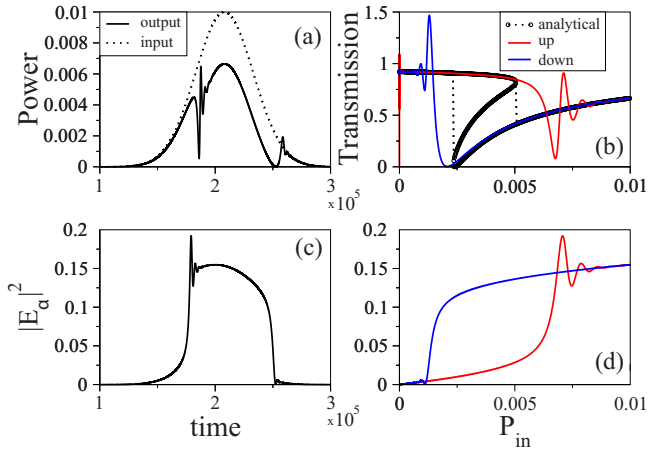

FIG. 4. (Color online) (a) Time evolution of the input (dashed line) and output (solid line) pulses. (b) Transmission coefficients, derived from (a) (red and blue curves) and the analytical one for this system [2]. (c) Time evolution of the nonlinear cavity excitation. (d) The effective pumping rate of the cavity, derived from (c). The parameters of the system are $\epsilon_n=\epsilon_\alpha=2.56$, the frequency is $\Omega=0.373$ [see Fig. 1(c)]. The parameters of the Gaussian pulse are $I_1=0.1$, $t_0=2\times10^5$, and $w=5\times10^4$.

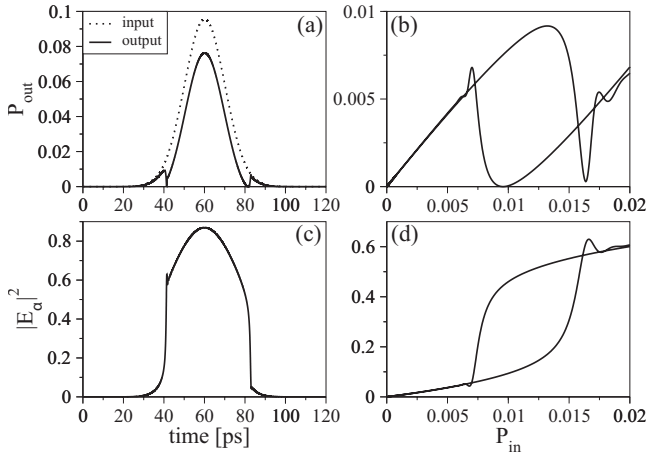

FIG. 5. Results of the direct FDTD simulations of the structure described in the text. These results should be compared to Fig. 4. (a) Shape of the input (dashed) and output (solid line) pulses. (b) Output power P_{out} versus input power P_{in} derived from (a). (c) Temporal evolution of the side-coupled nonlinear cavity excitation. (d) The effective pumping rate of the cavity, derived from (c).

$$\tilde{E}_n(T|\Omega)=e^{-i\nu T}\begin{cases} Ie^{iq(\Omega)n}+r(T)e^{-iq(\Omega)n}, & n\ll 0,\\ t(T)e^{iq(\Omega)n}, & n\gg 0.\end{cases} \tag{11}$$

By using the fact that Eqs. (10) for the straight waveguide are linear and that the expression for the continuous-wave excitation is known, $Ie^{i[q(\Omega)n-\nu T]}$, we can rewrite the system (10) after some algebraic manipulation in the form

$$-i\sigma\frac{\partial}{\partial T}\tilde{E}_n=V_{0,1}(\Omega)(\tilde{E}_{n-1}+\tilde{E}_{n+1})\sum_{l=n_1}^{n_2}\delta_{n,l}V_{l-n_1,\alpha}\tilde{E}_\alpha,$$

$$n<-1,\quad n>0,$$

$$-i\sigma\frac{\partial}{\partial T}\tilde{E}_{-1}=V_{0,1}(\Omega)(\tilde{E}_{-2}+\tilde{E}_0)-V_{0,1}(\Omega)Ie^{-i\nu T},$$

$$-i\sigma\frac{\partial}{\partial T}\tilde{E}_0=V_{0,1}(\Omega)(\tilde{E}_{-1}+\tilde{E}_1)+V_{0,1}(\Omega)Ie^{-iq(\Omega)-i\nu T},$$

$$-i\sigma\frac{\partial}{\partial T}\tilde{E}_\alpha=\kappa_\alpha(\Omega)\chi_\alpha^{(3)}|\tilde{E}_\alpha|^2\tilde{E}_\alpha+[D_n(\Omega)-D_\alpha(\Omega)]\tilde{E}_\alpha$$

$$+\sum_{l=n_1}^{n_2}V_{\alpha,l-n_1}\tilde{E}_l, \tag{12}$$

with the explicit time-periodic parametric excitations at the sites $n=-1,0$, which mimic the continuous-wave mode propagating to the right, $n>0$. As a result, the rescaled electric field $\tilde{E}_n$ describes now the reflected ($n\ll0$) and transmitted ($n\gg0$) waves only.

In such a form, the system (12) can be solved numerically, with a high efficiency, by using the *discrete transparent boundary conditions* method [37]. The main advantage of this method is that it allows one to reduce significantly the spatial domain of the system to a few sites, thus reducing drastically the required computation time.

IV. MODULATIONAL INSTABILITY

The system we have derived above is rather general, and it can be applied to many types of low-loss waveguide-resonator structures under the assumption of a weak coupling. As a specific example, below we consider a two-dimensional photonic crystal created by a lattice of dielectric rods of radius $r_{rod}=0.18a$ with permittivity $\epsilon_r=11.56$, where a is the lattice period. This structure is known to support a large TM band gap [32].

We study the so-called on-site geometry [2] with three coupling terms describing the interaction with the nonlinear cavity, with $n_1=-1$ and $n_2=1$ in Eqs. (7)–(11), as shown in Fig. 1(b).

The steady-state solutions of Eq. (8) were obtained earlier in Ref. [2]. Figure 1(c) represents the typical shape of the linear Fano resonance for small input intensities. In this paper, we are interested in the dynamics of the scattering process. First, we perform a stability analysis of the continuous-wave scattering near the nonlinear Fano resonance. We linearize the system (8) near the steady-state solutions, $E_n=E_n'+\phi_n$, by adding a small perturbation $|\phi_n|\ll|E_n'|$, and study the eigenvalue spectrum of the linearized system ϕ_n. The real eigenvalues correspond to stable solutions, while the presence of complex conjugated pairs indicates that a given solution is dynamically unstable and will diverge exponentially with time. Our analysis suggests that even in the case when there is no bistability the continuous wave can become dynamically unstable near the nonlinear Fano resonance, as indicated in Fig. 2(b) by the complex eigenvalues. A similar scenario was predicted in Ref. [38], where it was shown that it corresponds to generic modulational instability in nonlinear systems.

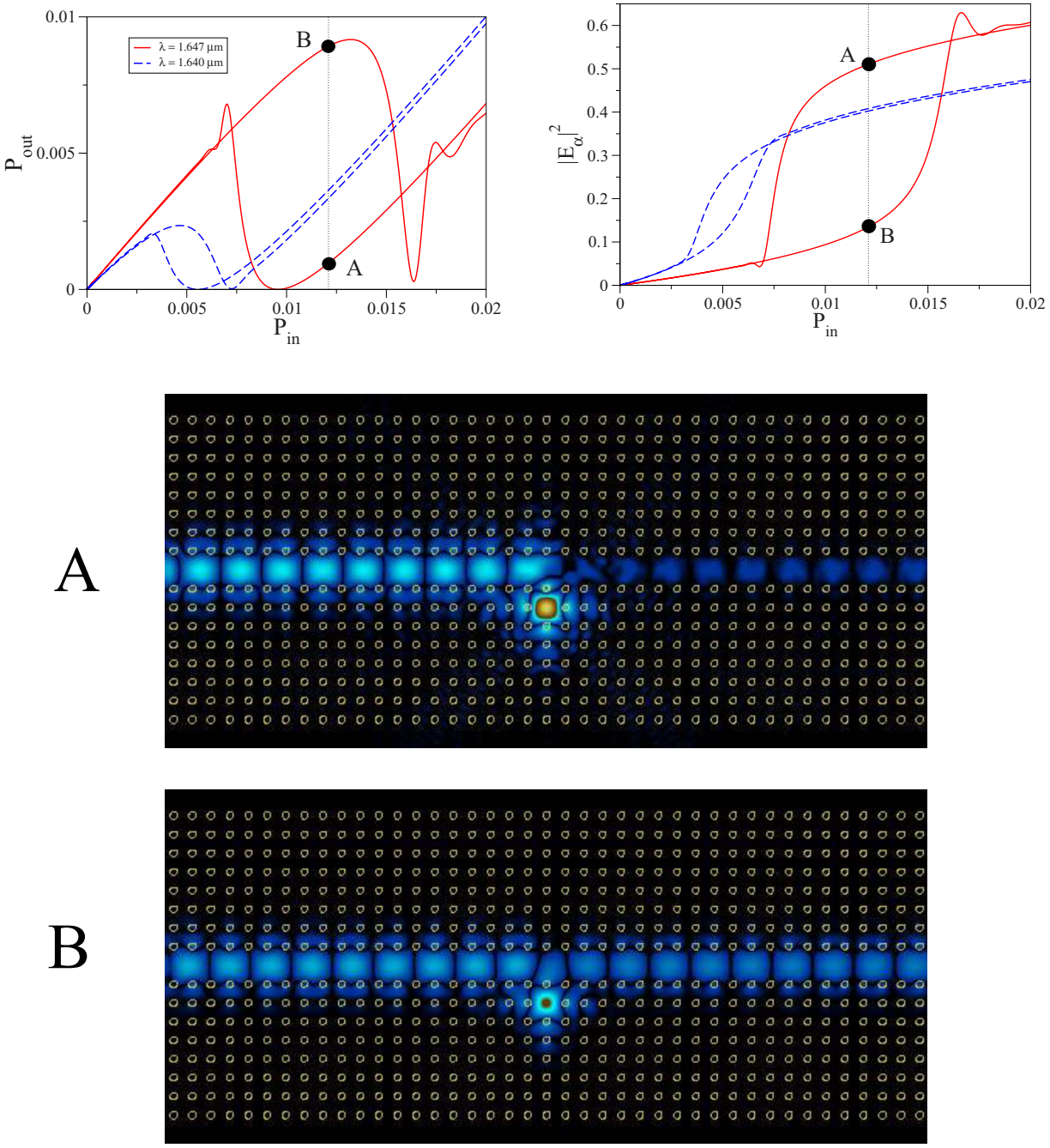

FIG. 6. (Color online) Output power P_{out} (left) and pumping rate of the cavity (right) versus input power P_{in} for two detuning wavelengths, $\lambda=1647$ nm (optimal) and $\lambda=1640$ nm. For the optimal case ($\lambda=1647$ nm) electric field profiles near the nonlinear resonance ($P_{in}=0.0121$) are given for the two stable branches (A and B).

In Fig. 3 the temporal evolution of the electric field in the cavity is displayed, for two cases: (i) at resonance, $P_{in}=0.1252$ [see Figs. 3(a) and 3(b)], and (ii) far from resonance, $P_{in}=0.01$ [see Figs. 3(c) and 3(d)]. The development of *modulational instability* of the electric field in the cavity near the resonance condition is clearly visible [see Fig. 3(a)], where the intensity of the field starts to grow with time. Initially this is an exponential growth, but after a transition the growth is even faster. The transition time can be estimated from the maximum value of the imaginary part of the unstable eigenvalue [see Fig. 2(b)]. Far from resonance, we observe saturation of the field in the cavity, as shown in Fig. 3(c). It corresponds to a stable regime.

It is interesting to look at the temporal evolution of the transmission coefficient for both cases [see Figs. 3(b) and 3(d)]. Even in the presence of modulational instability, the transmission coefficient is well defined. It shows the transition from 0 (resonant condition) to 1 [see Fig. 3(b)]. Despite the fact that the field in the cavity grows, the system is almost transparent. In the stable case, far from resonance [see Fig. 3(d)], the transmission coefficient simply reaches the steady-state value predicted theoretically [2].

V. PULSE SCATTERING

To address the question whether a bistable transmission is possible in this system, we consider the same problem for a nonstationary, pulsed excitation. This issue is important because the modulational instability we found above requires a certain time to develop [see Fig. 3(a)]. We expect that in the nonstationary transmission regime the instability may be suppressed or even eliminated. We notice that for very short pulses, we may enter the regime of chaotic dynamics of the system, and we use relatively broad Gaussian pulses,

$$I = I_1 \exp\left(-\frac{(T-T_0)^2}{w^2}\right), \tag{13}$$

where w is the pulse width.

Our results are presented in Fig. 4, and they show that for long pulses we are able to reproduce the whole bistable curve predicted by the stationary scattering analysis [2]. The input and output profiles are shown in Fig. 4(a). From these temporal profiles we can obtain the transmission coefficient, as shown in Fig. 4(b). The results of the dynamical simulations (red and blue curves) are in a perfect agreement with the theoretical (analytical) results shown by black curves. The oscillations in the transmission come from the fact that one of the stable solutions ceases to exist, and the system jumps to another stable state. This switching is accompanied by a critical slowing down close to the critical points of the bifurcation curve. Such a dynamical sweeping of the input parameter leads to an increased area of the hysteresis loop, depending on the modulation speed, as was earlier discussed in Ref. [39] in a different context. Figures 4(c) and 4(d) show the time evolution of the cavity excitation and effective pumping rate, respectively. The excitation of the cavity varies up to two orders of magnitude within the hysteresis loop.

Finally, we have performed direct FDTD simulations to check our theoretical predictions. For this purpose we consider a two-dimensional square photonic crystal of silicon rods in air of radius $r_{\mathrm{rod}}=108$ nm with $\epsilon_r=11.56$. The period of the structure is $a=600$ nm. We construct a photonic crystal waveguide by removing one row of rods. For the side-coupled cavity one rod at $2a$ distance from the waveguide is replaced by a polymer one with the same rod radius r_{rod}, whose permittivity is $\epsilon_\alpha=2.56$. In the linear regime, such a structure supports a Fano resonance (total reflection) at $\lambda=1628$ nm, with a quality factor $Q=118$.

In Fig. 5, our FDTD results for Gaussian pulse propagation in the nonlinear regime are presented for detuned wavelength at $\lambda=1647$ nm. These results are in excellent agreement with the theoretical ones, presented in Fig. 4.

In Fig. 6 we show how the bistable region changes for different detuning wavelengths $\lambda=1647$ nm (optimal) and $\lambda=1640$ nm. Moreover, the electric field profiles near the nonlinear resonance are plotted for two stable branches at a given power $P_{\mathrm{in}}=0.0121$.

VI. CONCLUSIONS

We have studied analytically the dynamics of nonlinear Fano resonances observed in the propagation of linear guided modes coupled to a localized mode of a nonlinear resonant cavity. We have revealed the existence of modulational instability for the nonlinear Fano resonance that manifests itself in a growth of the light intensity in the cavity. For the specific case of a photonic crystal created by a two-dimensional lattice of dielectric rods in air, we have derived the effective discrete equations for the nonlinear scattering problem, employing the time-dependent version of the Green's function formalism, and studied analytically the reflectivity of continuous waves and linear stability of the corresponding stationary scattering problem. We have found that modulational instability that occurs near the nonlinear Fano resonance is largely suppressed for Gaussian pulses and that is why it is readily possible to recover the bistable transmission curves in the pulse regime. Our analytical predictions are in excellent agreement with the numerical results obtained by FDTD simulations. Although derived in the context of photonic-crystal-based waveguides and cavities, the approach developed here can be useful for the study of other types of low-loss waveguide-resonator structures.

ACKNOWLEDGMENTS

This work has been supported by the Deutsche Forschungsgemeinschaft (Research Unit 532), the German Federal Ministry of Education and Research (Innoregio, ZIK), and the Australian Research Council. Y.K. and R.I. gratefully acknowledge support from the Carl Zeiss Foundation. The authors thank Shanhui Fan and Sergei Mingaleev for useful discussions and comments.

[1] S. Fan, Appl. Phys. Lett. **80**, 908 (2002).
[2] S. F. Mingaleev, A. E. Miroshnichenko, Yu. S. Kivshar, and K. Busch, Phys. Rev. E **74**, 046603 (2006).
[3] U. Fano, Phys. Rev. **124**, 1866 (1961).
[4] K. Kobayashi, H. Aikawa, S. Katsumoto, and Y. Iye, Phys. Rev. Lett. **88**, 256806 (2002).
[5] J. U. Nöckel and A. D. Stone, Phys. Rev. B **50**, 17415 (1994).
[6] J. Göres, D. Goldhaber-Gordon, S. Heemeyer, M. A. Kastner, H. Shtrikman, D. Mahalu, and U. Meirav, Phys. Rev. B **62**, 2188 (2000).
[7] B. R. Bulka and P. Stefanski, Phys. Rev. Lett. **86**, 5128 (2001).
[8] M. E. Torio, K. Hallberg, S. Flach, A. E. Miroshnichenko, and M. Titov, Eur. Phys. J. B **37**, 399 (2004); A. A. Aligia and L. A. Salguero, Phys. Rev. B **70**, 075307 (2004).
[9] S. Noda, A. Chutinan, and M. Imada, Nature (London) **407**, 608 (2000).
[10] S. Fan and J. D. Joannopolos, Phys. Rev. B **65**, 235112 (2002).
[11] M. F. Yanik, S. Fan, and M. Soljačić, Appl. Phys. Lett. **83**,

2739 (2003).
[12] A. R. Cowan and J. F. Young, Phys. Rev. E **68**, 046606 (2003).
[13] S. Fan, W. Suh, and J. D. Joannopoulos, J. Opt. Soc. Am. A **20**, 569 (2003).
[14] V. Lousse and J. P. Vigneron, Phys. Rev. B **69**, 155106 (2004).
[15] A. E. Miroshnichenko and Yu. S. Kivshar, Opt. Express **13**, 3969 (2005).
[16] S. F. Mingaleev, A. E. Miroshnichenko, and Yu. S. Kivshar, Opt. Express **15**, 12380 (2007).
[17] S. F. Mingaleev, A. E. Miroshnichenko, and Yu. S. Kivshar, Opt. Express **16**, 11647 (2008).
[18] R. Iliew, C. Etrich, U. Peschel, and F. Lederer, IEEE J. Sel. Top. Quantum Electron. **12**, 377 (2006).
[19] R. Iliew, C. Etrich, M. Augustin, E.-B. Kley, S. Nolte, A. Tünnermann, and F. Lederer, Phys. Status Solidi A **204**, 3689 (2007).
[20] X. Yang, C. Husko, C. W. Wong, M. Yu, and Dim-Lee Kwong, Appl. Phys. Lett. **91**, 051113 (2007).
[21] B. Maes, P. Bienstman, and R. Baets, Opt. Express **16**, 3069 (2008).
[22] E. Tekman and P. F. Bagwell, Phys. Rev. B **48**, 2553 (1993).
[23] S. W. Kim and S. Kim, Phys. Rev. B **63**, 212301 (2001).
[24] S. Flach, A. E. Miroshnichenko, V. Fleurov, and M. V. Fistul, Phys. Rev. Lett. **90**, 084101 (2003).
[25] S. Noda, A. Chutinan, and M. Imada, Nature (London) **407**, 608 (2000).
[26] T. Asano, B. S. Song, Y. Tanaka, and S. Noda, Appl. Phys. Lett. **83**, 407 (2003).
[27] M. Notomi, A. Shinya, S. Mitsugi, G. Kira, E. Kuramochi, and T. Tanabe, Opt. Express **13**, 2678 (2005).
[28] P. E. Barclay, K. Srinivasan, and O. Painter, Opt. Express **13**, 801 (2005).
[29] X. Yang, C. Husko, C. W. Wong, M. Yu, and D.-L. Kwong, Appl. Phys. Lett. **91**, 051113 (2007).
[30] A. Taflove and S. C. Hagness, *Computational Electrodynamics: The Finite-Difference Time-Domain Method* (Artech House, Boston, MA, 2005).
[31] S. F. Mingaleev and Yu. S. Kivshar, Opt. Lett. **27**, 231 (2002).
[32] S. F. Mingaleev and Yu. S. Kivshar, J. Opt. Soc. Am. B **19**, 2241 (2002).
[33] S. F. Mingaleev and Yu. S. Kivshar, Phys. Rev. Lett. **86**, 5474 (2001).
[34] A. J. Ward and J. B. Pendry, Phys. Rev. B **58**, 7252 (1998).
[35] A. E. Miroshnichenko, S. F. Mingaleev, S. Flach, and Yu. S. Kivshar, Phys. Rev. E **71**, 036626 (2005).
[36] S. F. Mingaleev, Yu. S. Kivshar, and R. A. Sammut, Phys. Rev. E **62**, 5777 (2000).
[37] A. Arnold, M. Ehrhardt, and I. Sofronov, Commun. Math. Sci. **1**, 501 (2003).
[38] B. A. Malomed and M. Ya. Azbel, Phys. Rev. B **47**, 10402 (1993).
[39] P. Jung, G. Gray, R. Roy, and P. Mandel, Phys. Rev. Lett. **65**, 1873 (1990).